Journal of Applied Physics

A quantum model for photoemission from metal surfaces and its comparison with the three-step model and Fowler–DuBridge model

Cite as: J. Appl. Phys. **127**, 164903 (2020); https://doi.org/10.1063/5.0004140
Submitted: 07 February 2020 . Accepted: 08 April 2020 . Published Online: 24 April 2020

Yang Zhou, and Peng Zhang

AIP Publishing

Journal of Applied Physics ARTICLE scitation.org/journal/jap

A quantum model for photoemission from metal surfaces and its comparison with the three-step model and Fowler–DuBridge model

Cite as: J. Appl. Phys. **127**, 164903 (2020); doi: 10.1063/5.0004140
Submitted: 7 February 2020 · Accepted: 8 April 2020 ·
Published Online: 24 April 2020

View Online Export Citation CrossMark

Yang Zhou and Peng Zhang[a)]

AFFILIATIONS

Department of Electrical and Computer Engineering, Michigan State University, East Lansing, Michigan 48824-1226, USA

[a)]**Author to whom correspondence should be addressed:** pz@egr.msu.edu

ABSTRACT

This paper studies a quantum mechanical model for photoemission from a metal surface due to the excitation of laser electric fields, which was developed by solving the time-dependent Schrödinger equation exactly. The quantum model includes the effects of laser fields (wavelength and intensity), properties of metals (Fermi energy and work function including Schottky effect), and the applied dc field on the cathode surface. Shorter wavelength lasers can induce more photoemission from electron initial energy levels further below the Fermi level and, therefore, yield larger quantum efficiency (QE). The dc field increases QE, but it is found to have a greater impact on lasers with wavelengths close to the threshold (i.e., the corresponding photon energy is the same as the cathode work function) than on shorter wavelength lasers. The quantum model is compared with existing classical models, i.e., the three-step model, the Fowler–DuBridge model, and the Monte Carlo simulation based on the three-step model. Even though with very different settings and assumptions, it is found that the scaling of QE of the quantum model agrees well with other models for low intensity laser fields. When the laser field increases, QE increases with the laser field strength in the longer laser wavelength range due to the increased contributions from multiphoton absorption processes.

I. INTRODUCTION

Laser-driven photoelectron emission is important to photoinjectors in free electron lasers and accelerators,[1,2] ultrafast electron microscopes,[3] x-ray sources,[4] femtosecond electron diffraction,[5] and novel vacuum nanoelectronics.[6–8] The mechanisms of laser-driven photoemission from metal surfaces have been studied extensively both theoretically and experimentally.[2,9–16] For decades, the fundamental models of photoemission remain those of classical treatment models, such as the three-step model (TSM)[13–18] and the Fowler–DuBridge (FD) model.[9–12] There have also been recent interests in multi-photon absorption induced over-barrier emission for weak laser fields, photon-assisted tunneling, and optical field tunneling emission for strong laser fields.[19–23] Quantum treatments of the photoemission from metal surfaces assume that the free electrons inside the metal are confined by a step potential barrier, which can be modulated by a dc field or a laser field.[24] Recently, an analytical model for electron emission from metal surfaces due to the arbitrary combination of dc electrical field and laser electric field was constructed by solving the time-dependent Schrödinger equation exactly.[22] The model has been extended to two-color laser induced electron emission.[25,26] It includes the effects of lasers (wavelength and intensity), dc electric field, and metal properties (work function and Fermi level). However, it only considers electrons with initial energy at the Fermi level, without considering the contribution of photoemission from electrons with other initial energies inside the cathode.

Here, we extend the quantum model (QM) for photoemission based on the exact solution of the time-dependent Schrödinger equation to include the effects of electron energy states' distribution inside the metal, which is assumed to follow the Fermi–Dirac distribution. Electron emission mechanisms under various conditions are analyzed. The quantum efficiency (QE), defined as the number of emitted electrons per incident photon, is calculated from our quantum model. The results are compared with the three-step model [both the Dowell's analytical model[17,18] and a simple Monte Carlo (MC) simulation] and the Fowler–DuBridge model.

II. QUANTUM MODEL FOR PHOTOEMISSION

A. Formulation

Consider a one-dimensional (1D) model[22,25,26] as shown in Fig. 1, in which it is assumed that electrons with initial energy ε are emitted from the metal–vacuum interface at $x=0$, under the action of both a laser field $F_1\cos\omega t$ and a dc field F_0, where F_1 is the magnitude of the laser field and ω is the frequency of the laser. The laser field is assumed to be perpendicular to the interface and cut off abruptly at the surface. This assumption may be justified by that the laser penetration depth is much smaller than the laser wavelength. Thus, the time-dependent surface potential barrier is[22,25,26]

$$\Phi(x,t)=\begin{cases}0, & x<0,\\ E_F+W-eF_0x-eF_1x\cos\omega t, & x\geq 0,\end{cases} \tag{1}$$

where E_F is the Fermi level of the metal, $W=W_0-2\sqrt{e^3F_0/16\pi\varepsilon_0}$ is the effective work function including the potential barrier lowering by the Schottky effect due to the dc electric field F_0, W_0 is the metal work function, e is the electron charge, and ε_0 is the free space permittivity. Note that, though Eq. (1) assumes a linear potential in order to yield an analytical solution, it has been verified in Ref. 22 that this approach gives a very good approximation of the more realistic nonlinear potential including image charge.[27] Due to the omission of the laser penetration inside the metal, the effects of electron–electron scattering and electron–phonon scattering, which may happen when electrons inside the metal move to the surface, are also ignored in this model.

The electron wave function $\psi(x,t)$ can be solved from the time-dependent Schrödinger equation,

$$i\hbar\frac{\partial\psi(x,t)}{\partial t}=-\frac{\hbar^2}{2m}\frac{\partial^2\psi(x,t)}{\partial x^2}+\Phi(x,t)\psi(x,t), \tag{2}$$

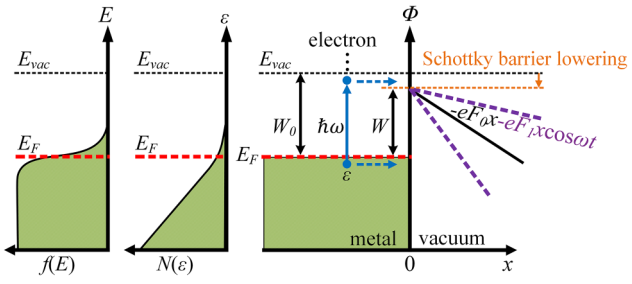

FIG. 1. Energy diagram for laser-driven photoelectron emission from a metal surface with dc bias. The metal has Fermi level E_F and original work function W_0. The dc field is F_0, and the laser electric field is $F_1\cos\omega t$, both of which are assumed perpendicular to the metal surface. The effective work function $W=W_0-2\sqrt{e^3F_0/16\pi\varepsilon_0}$ with the Schottky effect. Left: Electrons inside the metal are assumed to follow the three-dimensional Fermi–Dirac distribution $f(E)$. Center: The corresponding one-dimensional electron supply function with longitudinal energy $\varepsilon=E_x$ is $N(\varepsilon)$ [cf. Eq. (9)]. Right: The oscillating potential barrier due to laser and dc fields.

where $\hbar$ is the reduced Planck's constant, m is the electron mass, and $\Phi(x,t)$ is the laser field modulated surface potential barrier given in Eq. (1).

For $x<0$, the solution to Eq. (2) is

$$\psi(x,t)=e^{-i\frac{\varepsilon}{\hbar}t+ik_0x}+\sum_{n=-\infty}^{\infty}R_ne^{-i\frac{\varepsilon+n\hbar\omega}{\hbar}t-ik_nx}, \tag{3}$$

where ε is the electron initial energy and R_n is the reflection coefficient of the incident electron wave. Equation (3) is the superposition of incident electron wave with the wave vector of $k_0=\sqrt{2m\varepsilon/\hbar^2}$, and reflected electron waves from the metal–vacuum interface with the wave vector of $k_n=\sqrt{2m(\varepsilon+n\hbar\omega)/\hbar^2}$.

Taking the Truscott transformation,[28] the exact solution to Eq. (2) for $x\geq 0$ is found to be[22,25,26]

$$\psi(x,t)=\begin{cases}\sum_{n=-\infty}^{\infty}T_ne^{i\sqrt{\frac{2mE_n}{\hbar^2}}\xi}\Theta(x,t), & F_0=0,\\ \sum_{n=-\infty}^{\infty}T_nG_n(x,t)\Theta(x,t)e^{-\frac{ie^2F_0F_1\sin\omega t}{\hbar m\omega^3}}, & F_0\neq 0,\end{cases} \tag{4}$$

where T_n is the electron wave transmission coefficient, $\xi=x+(eF_1/m\omega^2)\cos\omega t$, $E_n=\varepsilon+n\hbar\omega-E_F-W-U_p$ with $U_p=e^2F_1^2/4m\omega^2$, $\Theta(x,t)=\exp\left(-i\frac{\varepsilon+n\hbar\omega}{\hbar}t+\frac{ieF_1\sin\omega t}{\hbar\omega}x+\frac{ie^2F_1^2\sin 2\omega t}{8\hbar m\omega^3}\right)$, $G_n(x,t)=Ai(-\eta_n)-iBi(-\eta_n)$ with $\eta_n=(E_n/eF_0+\xi)(2emF_0/\hbar^2)^{1/3}$, and Ai and Bi are the Airy function of the first and second kind. Equation (4) is the transmitted electron wave traveling to the vacuum side, and it is the superposition of electron waves with the energy of $\varepsilon+n\hbar\omega$ induced by different emission mechanisms, namely, multiphoton absorption ($n>0$), tunneling ($n=0$), and multiphoton emission ($n<0$).[22,25,26]

Using boundary conditions that both $\psi(x,t)$ and $\partial\psi(x,t)/\partial x$ are continuous at $x=0$ and taking the Fourier transform, we obtain, in the normalized form,

$$2\sqrt{\bar{\varepsilon}}\delta(l)=\sum_{n=-\infty}^{\infty}T_n\left(\sqrt{\bar{\varepsilon}+l\bar{\omega}}P_{n(n-l)}+Q_{n(n-l)}\right), \tag{5}$$

where δ is the Dirac delta function, $P_{nl}=1/2\pi\times\int_0^{2\pi}p_n(\bar{\omega}\bar{t})e^{-il\bar{\omega}\bar{t}}d(\bar{\omega}\bar{t})$ and $Q_{nl}=1/2\pi\times\int_0^{2\pi}q_n(\bar{\omega}\bar{t})e^{-il\bar{\omega}\bar{t}}d(\bar{\omega}\bar{t})$ are the Fourier transform coefficients, with

$$p_n(\bar{\omega}\bar{t})=e^{\frac{i\bar{F}_1^2}{4\bar{\omega}^3}\sin 2\bar{\omega}\bar{t}}e^{i\frac{2\bar{F}_1}{\bar{\omega}^2}\sqrt{\bar{E}_n}\cos\bar{\omega}\bar{t}},\quad q_n(\bar{\omega}\bar{t})=p_n(\bar{\omega}\bar{t})\left[\sqrt{\bar{E}_n}+\frac{\bar{F}_1\sin\bar{\omega}\bar{t}}{\bar{\omega}}\right] \tag{6a}$$

for $F_0=0$, and

$$p_n(\bar{\omega}\bar{t})=z(\bar{\omega}\bar{t})s(\alpha_n),\quad q_n(\bar{\omega}\bar{t})=z(\bar{\omega}\bar{t})\left[\frac{\bar{F}_1\sin\bar{\omega}\bar{t}}{\bar{\omega}}s(\alpha_n)+\bar{F}_0^{\frac{1}{3}}r(\alpha_n)\right] \tag{6b}$$

for $F_0\neq 0$, with $z(\bar{\omega}\bar{t})=\exp\left(-\frac{i2\bar{F}_0\bar{F}_1}{\bar{\omega}^3}\sin\bar{\omega}\bar{t}+\frac{i\bar{F}_1^2}{4\bar{\omega}^3}\sin 2\bar{\omega}\bar{t}\right)$, $s(\alpha_n)=Ai(\alpha_n)-iBi(\alpha_n)$, $r(\alpha_n)=iAi'(\alpha_n)+Bi'(\alpha_n)$, and $\alpha_n=-[\bar{E}_n/\bar{F}_0+(2\bar{F}_1/\bar{\omega}^2)$

$\cos(\bar{\omega}\bar{t})]\overline{F_0}^{\frac{1}{3}}$. A prime denotes the derivative with respect to its argument. The quantities with a bar are in their normalized form, defined as $\bar{\varepsilon} = \varepsilon/W$, $\bar{\omega} = \hbar\omega/W$, $\bar{t} = tW/\hbar$, $\bar{x} = x/\lambda_0$, $\lambda_0 = \sqrt{\hbar^2/2mW}$, $\overline{F_0} = F_0 e\lambda_0/W$, $\overline{F_1} = F_1 e\lambda_0/W$, $\overline{E_F} = E_F/W$, $\overline{U_p} = U_p/W$, and $\overline{E_n} = E_n/W = \bar{\varepsilon} + n\bar{\omega} - \overline{E_F} - 1 - \overline{U_p}$. Therefore, the electron wave transmission coefficient T_n can be obtained from Eq. (5).

The probability of electron transmission can be calculated by $w(\varepsilon, x, t) = J_t(\varepsilon, x, t)/J_i(\varepsilon)$, where $J(\varepsilon, x, t) = (i\hbar/2m)(\psi\nabla\psi^* - \psi^*\nabla\psi)$, and J_i and J_t are the incident and transmitted electron probability current density, respectively. The time-averaged probability of electron transmission from initial energy of ε after n-photon process, $\langle w_n(\bar{\varepsilon})\rangle$, is

$$\langle w_n(\bar{\varepsilon})\rangle = \begin{cases} \mathrm{Im}\left(i\dfrac{\sqrt{\overline{E_n}}}{\sqrt{\bar{\varepsilon}}}|T_n|^2\right), & F_0 = 0, \\ \dfrac{\overline{F_0}^{1/3}}{\pi\sqrt{\bar{\varepsilon}}}|T_n|^2, & F_0 \neq 0, \end{cases} \tag{7}$$

and the total electron transmission probability $D(\bar{\varepsilon})$ from initial energy ε is the sum of $\langle w_n(\bar{\varepsilon})\rangle$,

$$D(\bar{\varepsilon}) = \sum_{n=-\infty}^{\infty} \langle w_n(\bar{\varepsilon})\rangle. \tag{8}$$

The emission current density can thereby be obtained by

$$J = e\int_0^{\infty} D(\varepsilon)N(\varepsilon)d\varepsilon, \tag{9}$$

where $D(\varepsilon)$ is given in Eq. (8) and $N(\varepsilon) = \frac{mk_BT}{2\pi^2\hbar^3}\ln\left(1 + e^{\frac{E_F-\varepsilon}{k_BT}}\right)$ is the supply function, with $N(\varepsilon)d\varepsilon$ being the flux of electrons inside the metal impinging on the metal surface with longitudinal energy between ε and $\varepsilon + d\varepsilon$ across a unit area per unit time, calculated from the free electron theory of metal.[29–31]

The quantum efficiency (QE) is defined as the ratio of the number of emitted electrons to that of incident photons,

$$QE = \frac{J/e}{I/\hbar\omega}, \tag{10}$$

where I is the intensity of the incident laser, which is related to the laser electric field as $I\,[\mathrm{W/cm^2}] = \varepsilon_0 cF_1^2/2 = 1.33\times10^{11}\times(F_1[\mathrm{V/nm}])^2$ for linearly polarized plane waves.

B. Transmission probability, current density, and quantum efficiency

Figure 2 shows the time-averaged electron transmission probability $\langle w_n(\varepsilon)\rangle$ through the n-photon process from copper, under various combinations of laser fields and wavelengths. The laser wavelengths for Figs. 2(a)–2(d) are 180 nm, 220 nm, 260 nm, and 280 nm, corresponding to the photon energy of 6.89 eV, 5.64 eV, 4.77 eV, and 4.43 eV, respectively. The applied dc field is 0. The laser fields F_1 for lines in purple, blue, green, and orange are 10 V/nm, 1 V/nm, 0.1 V/nm, and 0.01 V/nm, corresponding to the laser intensity of 1.33×10^{13}, 1.33×10^{11}, 1.33×10^{9}, and 1.33×10^{7} W/cm^2, respectively. The electron initial energy ε is assumed to be at the Fermi level E_F.

It is clear that the electron transmission probability through the nth channel increases when the laser field increases. The dominant emission process is through the single-photon absorption induced over-barrier emission ($n = 1$). Calculations with applied dc fields F_0 of up to 0.1 V/nm show F_0 has little effects on the transmission probability spectrum, indicating that the Schottky effect is negligible for such a small dc bias in the laser wavelength range of 180 nm –280 nm on copper cathodes.

The effects of laser fields F_1 (or laser intensity I), dc fields F_0, and laser wavelength λ on the total electron transmission probability $D(\varepsilon)$ from initial energy of E_F is shown in Fig. 3. For the relatively small applied dc field (up to 0.1 V/nm), the electron transmission probability is well scaled as $D(\varepsilon) \propto F_1^2$ for wavelengths shown in Fig. 3, indicating the dominant single-photon process. This is consistent with the characterization based on the Keldysh parameter $\gamma = \sqrt{W/2U_p} = \omega\sqrt{2mW}/eF_1$, which is used to characterize the transition from multiphoton absorption ($\gamma \gg 1$) to strong field emission ($\gamma \ll 1$). The smallest Keldysh parameter is $\gamma = 4.04$ when $F_1 = 12$ V/nm and $F_0 = 0.1$ V/nm at $\lambda = 260$ nm, implying that strong field photoemission can be neglected. When the laser wavelength increases from 180 nm to 260 nm, the

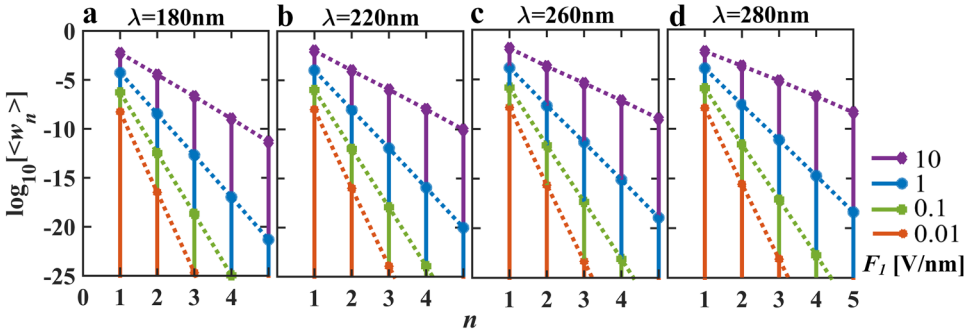

FIG. 2. Time-averaged electron transmission probability $\langle w_n(\varepsilon)\rangle$ through nth channel (or n-photon process) from electron initial energy $\varepsilon = E_F$ for laser wavelengths λ = (a) 180 nm, (b) 220 nm, (c) 260 nm, and (d) 280 nm, under various laser fields F_1 with dc field $F_0 = 0$. The metal is assumed to be copper, with $E_F = 7$ eV and $W_0 = 4.31$ eV. The laser intensity corresponding to the laser field F_1(V/nm) is $I\,[\mathrm{W/cm^2}] = \varepsilon_0 cF_1^2/2 = 1.33\times10^{11}\times(F_1[\mathrm{V/nm}])^2$.

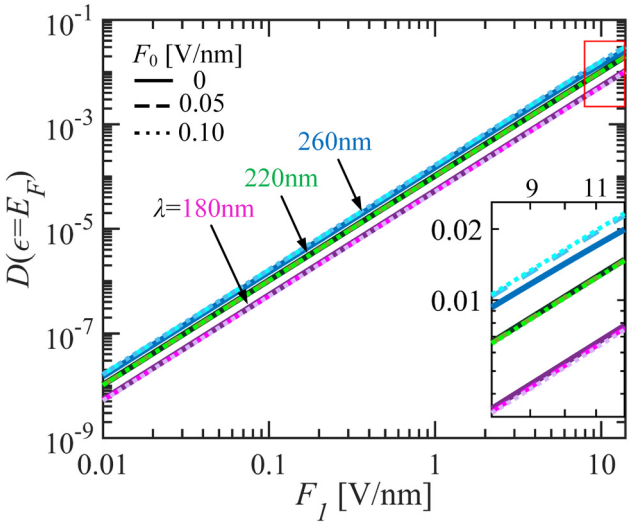

FIG. 3. The electron transmission probability $D(\varepsilon)$ at initial energy of E_F as a function of laser electric field F_1, for various laser wavelengths λ and dc field F_0. The metal is assumed to be copper, with $E_F = 7$ eV and $W_0 = 4.31$ eV.

corresponding photon energy decreases from 6.89 eV to 4.77 eV and becomes closer to the potential barrier seen by the electrons (i.e., $W \cong 4.31$ eV), leading to an increasing transmission probability $D(\varepsilon)$. This is consistent with our previous study that the maximum transmission occurs when the photon energy is equal to the potential barrier, $\hbar\omega/W \approx 1$ [cf. Fig. 6(c) of Ref. 22]. When the dc field increases, the potential barrier becomes narrower (Fig. 1), thus increasing the electron tunneling probability. In the meantime, the effective work function decreases because of the Schottky effect. The effects of the dc field are more pronounced for the longer laser wavelength (or smaller photon energy) of $\lambda = 260$ nm, as shown in the inset of Fig. 3. When the dc field is strong, e.g., $F_0 = 5$ V/nm, the dominant emission process becomes the dc field emission ($n = 0$) when the laser field is small, and electron transmission probability $D(\varepsilon = E_F)$ is independent of the laser wavelengths (not shown).

The electron transmission probability $D(\varepsilon)$ at different initial electron energy ε is shown in Fig. 4. The solid curves, which give $D(\varepsilon)$ as a function of ε at various laser fields, show a stair-like behavior. Each stair indicates a specific n-photon absorption for electrons with initial energy in that range. The energy between step points corresponds to the laser photon energy $\hbar\omega$. Take Fig. 4(a)-(ii), (v), and (viii) for $\lambda = 220$ nm as an example, whose projections in the D–ε plane and in the D–F_1 plane for a few selected curves are shown in Figs. 4(b) and 4(c), respectively. When $F_0 = 0$, the first step point is at $\varepsilon = 5.67$ eV [Fig. 4(b)], which equals $E_F + W_0 - \hbar\omega$, representing the electron initial energy threshold for one-photon emission. The second step point is near the bottom of the energy state. The difference between the two step points is 5.64 eV, which is the photon energy of the 220 nm laser. Electrons with initial energy in this range emit through two-photon absorption. The transmission probability $D(\varepsilon)$ of electrons with initial energy ε in the same stair range keeps almost constant under the same laser field F_1, only with a slight decrease as ε increases in that stair range. The difference in $D(\varepsilon)$ between stairs decreases when F_1 increases. For a given F_1, when the applied dc field F_0 increases, the step point shifts to smaller ε, because the surface potential barrier (or effective work function) is lowered by the applied dc field. The transition between stairs becomes gradual when there is dc field instead of a sharp transition when there is no dc field. Figure 4(c) shows $D(\varepsilon)$ as a function of laser field F_1 with various electron initial energies when the laser wavelength is 220 nm. When the electron is with initial energy of 2 eV and 4 eV, $D(\varepsilon)$ is well scaled as $D(\varepsilon) \propto F_1^{2n} = F_1^4$ for the applied dc field up to 0.1 V/nm, indicating the dominant two-photon absorption process. When the electron is with an initial energy of 5 eV, the dominant emission is through two-photon absorption for dc field smaller than 0.05 V/nm. When the applied dc field $F_0 = 0.1$ V/nm, which induces an effective work function of $W = 3.93$ eV, the effective potential barrier seen by an electron at $\varepsilon = 5$ eV becomes $E_F + W - \varepsilon = 5.93$ eV (compared to photon energy of 5.64 eV for a 220 nm laser). The electron is emitted through single-photon-assisted tunneling ($n = 1$) in the laser field range from $F_1 = 0.001$ V/nm to 1 V/nm. The dominant emission process shifts to high order channels ($n = 2$) when the laser field gets larger in the range from $F_1 = 1$ V/nm to 10 V/nm, as shown in Fig. 4(c), which is consistent with our previous observation (cf. Fig. 2 of Ref. 22).

Figure 5 presents the electron emission current density per energy $J(\varepsilon) = N(\varepsilon)D(\varepsilon)$ as a function of electron initial energy ε under various combinations of laser fields, dc fields, and laser wavelengths. Most electrons are emitted from electron initial energy of a few eVs below the Fermi level, through single-photon absorption. The range of the electron initial energy of single-photon emission is determined by the incident laser photon energy. The shorter the laser wavelength, the larger the range, and hence, more electrons are emitted. Few electrons above the Fermi level are emitted because there are fewer electrons distributed in that energy range. The dc field extends the dominant electron emission range to a lower value, and therefore more electrons with smaller initial energy are able to emit. The electron emission current density per energy $N(\varepsilon)D(\varepsilon)$ also shows stair-like dependence on the electron initial energy ε, indicating a different n-photon absorption process for electrons with initial energy in different "stairs." The step points correspond to the initial energy threshold for an electron to emit after absorption of integer number of photons $E_F + W - n\hbar\omega$. When the laser field F_1 increases, the electron emission current density also increases, but the difference of emission current density between stairs gets smaller, especially for longer laser wavelength, which means that a multi-photon absorption process contributes more significantly to the electron emission. When the laser field F_1 is small, as in Figs. 5(a)–5(c), the "stairs" are flat. When F_1 increases, $N(\varepsilon)D(\varepsilon)$ from larger initial energy becomes smaller than that from smaller initial energy in the same "stair," which is similar to the transmission probability $D(\varepsilon)$ observed in Fig. 4.

Figure 6 shows the total electron emission current density J as a function of laser wavelength under various laser fields, as calculated from Eq. (9). It is clear that when the laser field increases, the total emission current density also increases, especially in the

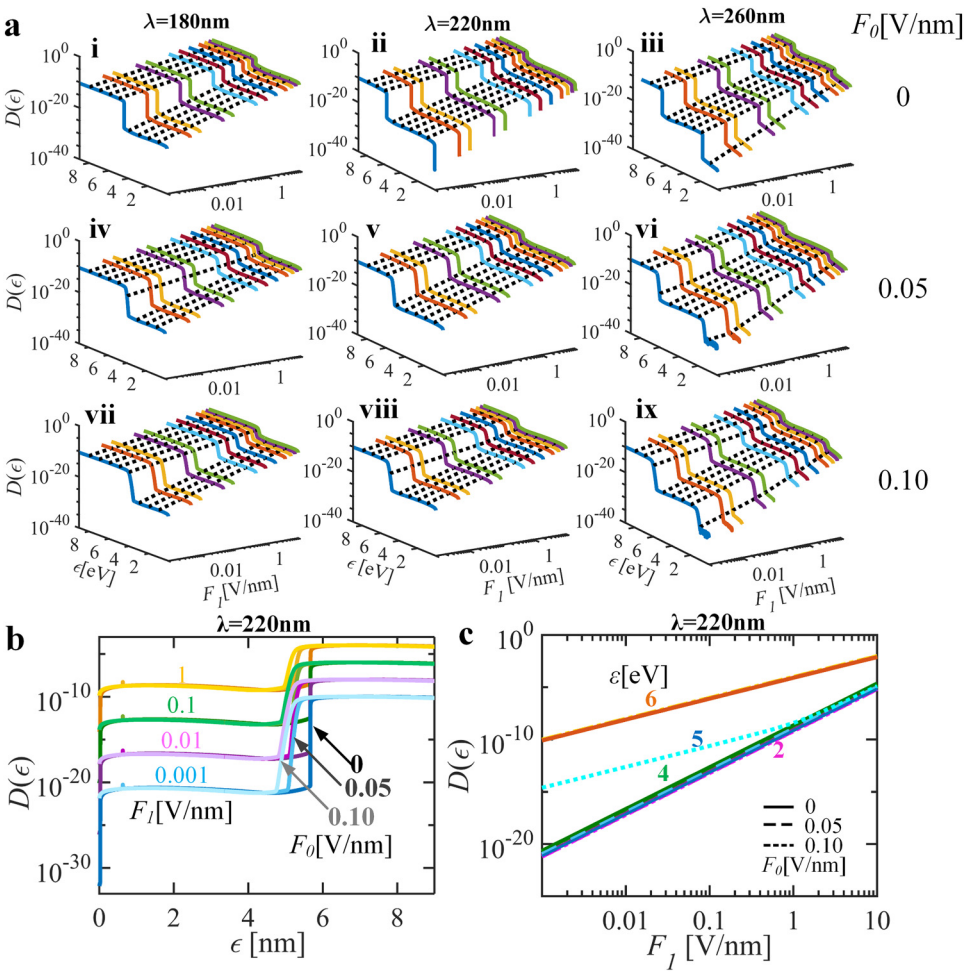

FIG. 4. Electron transmission probability $D(\varepsilon)$ as a function of electron initial energy ε, for different laser field F_1, dc field F_0, and laser wavelength λ. (a) Top to bottom row: $F_0 = 0$, 0.05, and 0.1 V/nm; Left to right column: $\lambda = 180$, 220, and 260 nm; (b) $D(\varepsilon)$ vs ε for $\lambda = 220$ nm; (c) $D(\varepsilon)$ vs F_1 for $\lambda = 220$ nm. The metal is assumed to be copper, with $E_F = 7$ eV and $W_0 = 4.31$ eV.

longer wavelength. When the laser field is small ($F_1 < 0.1$ V/nm), there is an obvious drop in the current density at a longer wavelength. When the laser field is larger, the electron emission current density becomes less sensitive to the laser wavelength. The application of dc field increases the total electron emission current density, due to both narrowing and lowering of the potential barrier. The increase of the emission current density due to the dc field is more significant for longer laser wavelength.

Regarding the high power of the laser used for photoemission, the temperature near the surface of the metal could increase substantially. The effects of temperature on the emission current are shown in Fig. 7. The laser field F_1 is 1 V/nm, and the temperature in the Fermi–Dirac function is set to be $T = 300$, 500, 1000, and 2000 K. It is clear that higher temperature can increase the emission current density in the longer laser wavelength range. As the electron temperature increases, there are more electrons near or above the Fermi level, which are able to emit and induce a larger emission current density. Electrons with initial energy above the Fermi level can emit through single-photon absorption in the longer laser wavelength range, whose transmission probability is several orders higher than electrons with lower energy (cf. Fig. 4). Therefore, the electron emission current density is greatly enhanced in the longer laser wavelength range. In the shorter laser wavelength range, electrons mostly emit through single-photon absorption over a wider range of initial energy around the Fermi level; therefore, the emission current density is insensitive to temperature.

Figure 8 shows quantum efficiency (QE) as a function of laser wavelength and laser field for different dc fields, as obtained from Eq. (10). For smaller laser wavelength in the range of 180 nm–260 nm, QE changes little when the laser field F_1 increases from 0 to 10 V/nm for a fixed dc field F_0. In this wavelength range, the electron emission is dominated by single-photon absorption, giving the scaling of the emission electron current density as $J \propto F_1^2$, or $J \propto I$, and thus a constant QE $\propto J/I$ independent of F_1, as seen from Figs. 8(c) and 8(f). For laser wavelength in the range of 260 nm–300 nm, QE increases when the input laser field F_1 increases. This is due to the increase in electron emission through multiphoton absorption ($n > 1$), as shown in Fig. 2. For the case of 300 nm, QE is increased by at least four orders of magnitude when

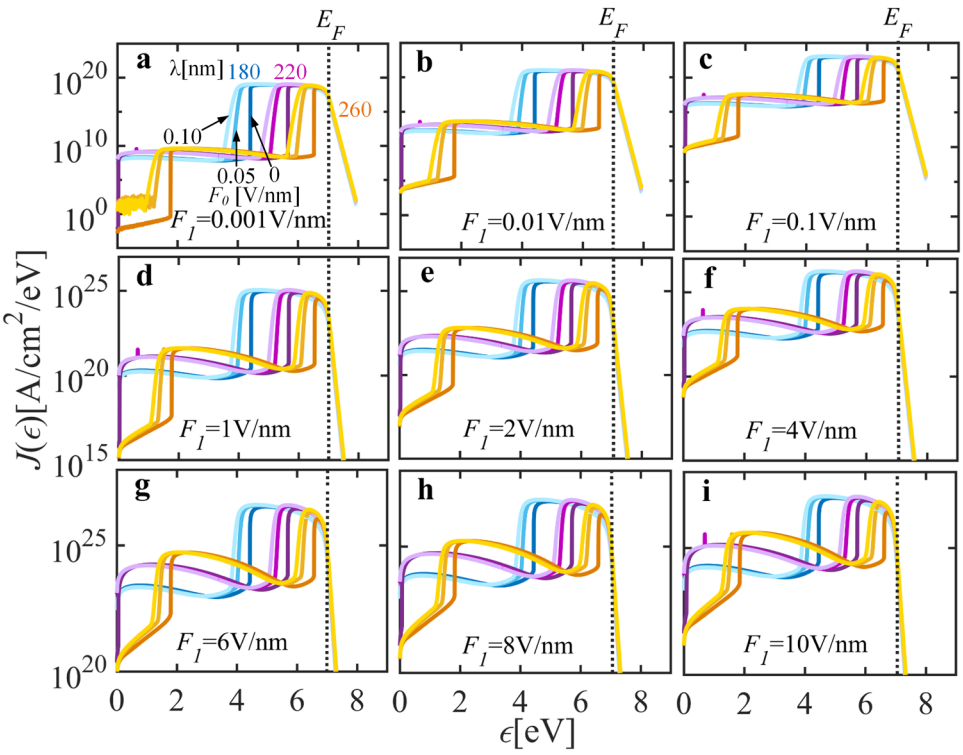

FIG. 5. Electron emission current density per electron initial energy $J(\varepsilon) = D(\varepsilon)N(\varepsilon)$ as a function of electron initial energy ε under various combinations of dc fields F_0 and wavelengths λ, for the laser field F_1 = (a) 0.001 V/nm, (b) 0.01 V/nm, (c) 0.1 V/nm, (d) 1 V/nm, (e) 2 V/nm, (f) 4 V/nm, (g) 6 V/nm, (h) 8 V/nm, and (i) 10 V/nm. The metal is assumed to be copper, with E_F = 7 eV and W_0 = 4.31 eV. The temperature is assumed at T = 300 K.

F_1 increases from 0.001 V/nm to 10 V/nm [cf. Fig. 8(c) with $F_0 = 0$), indicating that multiphoton absorption contributes significantly in this case. Applying a dc field will increase QE, as shown in Figs. 8(d)–8(f). The increase of QE due to the dc field is more profound in the longer laser wavelength range for a small laser field (e.g., λ in the range of 260 nm–300 nm with $F_1 < 1$ V/nm). It is also found that QE becomes less sensitive to the laser field F_1 when dc field F_0 is increased, especially for longer laser wavelength in 260 nm–300 nm.

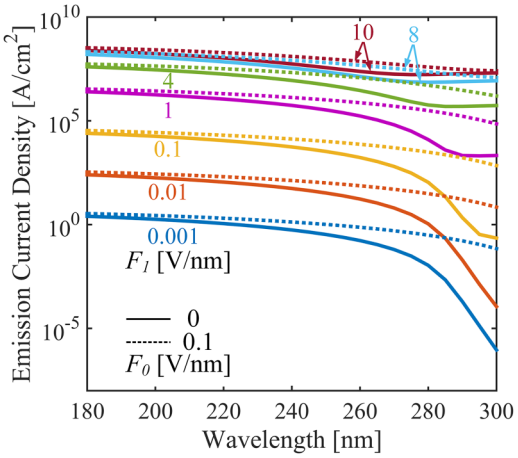

FIG. 6. Total electron emission current density as a function of laser wavelength under various laser fields F_1 and dc fields F_0. The metal is assumed to be copper, with E_F = 7 eV and W_0 = 4.31 eV. The electron temperature is assumed at T = 300 K.

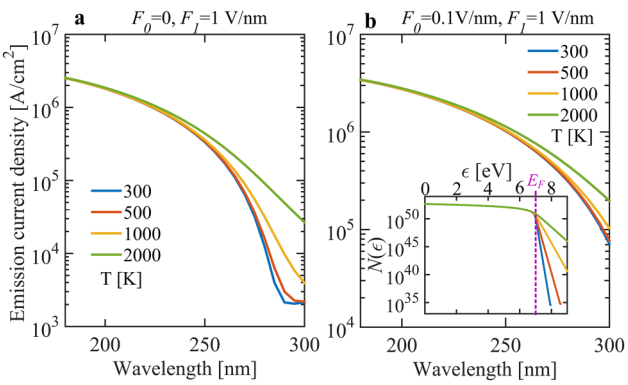

FIG. 7. Total electron emission current density as a function of laser wavelength with different temperatures. The laser field F_1 = 1 V/nm, and dc field F_0 = 0 for (a) and F_0 = 0.1 V/nm for (b). The inset in (b) is the supply function $N(\varepsilon)$ under various temperatures. The metal is assumed to be copper, with E_F = 7 eV and W_0 = 4.31 eV.

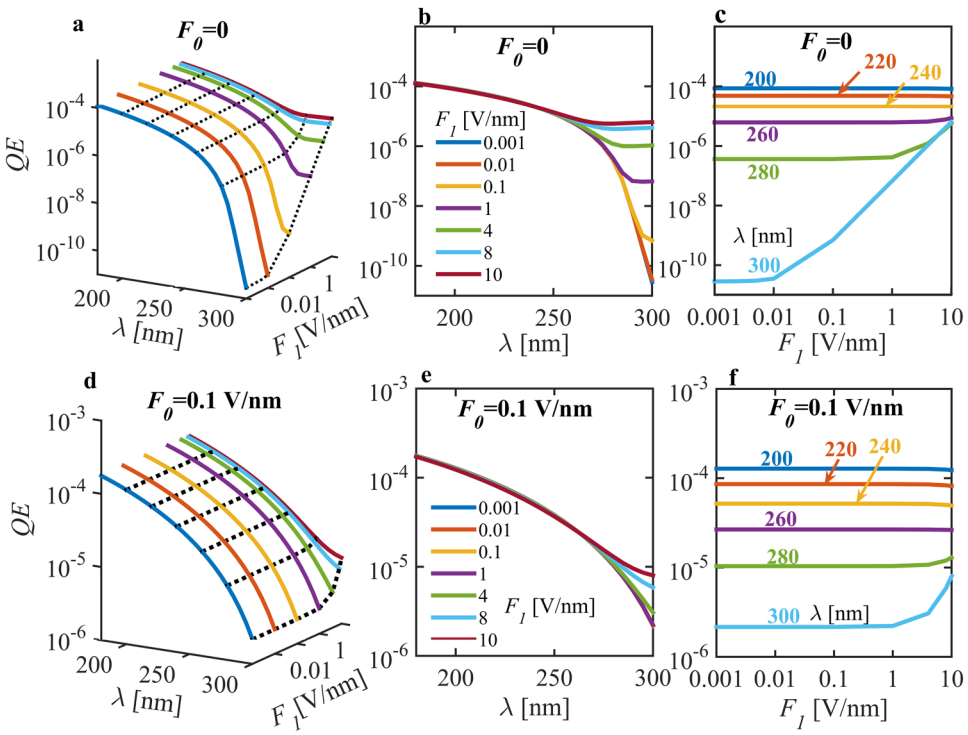

FIG. 8. Quantum efficiency calculated from the quantum model under various laser fields in the laser wavelength range of 180–300 nm for dc field F_0 of (a)–(c) 0 V/nm and (d)–(f) 0.1 V/nm. The metal is assumed to be copper, with $E_F = 7$ eV and $W_0 = 4.31$ eV. The temperature is assumed at $T = 300$ K.

III. COMPARISON WITH THE THREE-STEP MODEL AND THE FOWLER–DUBRIDGE MODEL

In this section, we compare the results of our quantum model with the widely used three-step model (TSM)[13–18] and the Fowler–DuBridge (FD) model.[9–12] The TSM in the closed form of Dowell[17,18] reads

$$\mathrm{QE} = (1 - R(\omega))F_{e-e}\frac{E_F + \hbar\omega}{2\hbar\omega}\left(1 - \sqrt{\frac{E_F + W}{E_F + \hbar\omega}}\right)^2, \quad \text{TSM}, \tag{11}$$

where $R(\omega)$ is the reflectivity at frequency ω, $(1 - R(\omega))$ is the laser power absorption coefficient, $F_{e-e}(\omega) = 1/\left(1 + \frac{\lambda_{opt}(\omega)}{\lambda_{e-e}(\omega)}\right)$, $\lambda_{opt}(\omega) = \lambda/4\pi k(\omega)$ is the optical penetration depth, λ is the laser wavelength and $k(\omega)$ is the imaginary part of the refractive index, and $\lambda_{e-e}(\omega) = \frac{2\lambda_m E_m^{3/2}}{\hbar\omega\sqrt{W}}\frac{1}{1+\sqrt{W/\hbar\omega}}$ is the mean free path of electron–electron scattering, with λ_m being a known value of electron–electron scattering mean free path for electrons at energy E_m above the Fermi level. Note that Eq. (11) is only a limiting case of TSM and is valid when the photon energy $\hbar\omega$ is close to the work function W of the metal. When $\hbar\omega$ is not close to W, scattered electrons with transverse energies and multiphoton processes may contribute greatly to the total emission and have to be considered in a more general three-step formalism.[32] The FD model[9–12] reads

$$\mathrm{QE} = a_1(1 - R(\omega))AT^2F\left(\frac{\hbar\omega - W}{k_BT}\right), \quad \text{FD model}, \tag{12}$$

where a_1 is a constant depending on the cathode material, $A = 120$ A/cm^2/K^2 is Richardson's constant, and $F(x)$ is Fowler's function [cf. Eq. (A5) in the Appendix]. For completeness, the assumptions in both models are briefly summarized in the Appendix.

Figures 9(a) and 9(b) show QE as a function of laser wavelength calculated by the quantum model [Eq. (10)], TSM [Eq. (11)], FD model [Eq. (12)], and Monte Carlo (MC) simulation based on TSM, for both copper and gold. In the calculation, the photon energy of the laser is chosen to be larger than the work function of the metal, such that the dominant electron emission mechanism is single-photon absorption. The laser field F_1 in the quantum model is assumed to be 0.01 V/nm. Though the absolute values for the QE from the quantum model are about one order smaller than those of the other models, their scalings are in remarkable agreement. In fact, by multiplying the QE from the quantum model with a constant C (=13.963 and 19.142 for copper and gold, respectively), it matches the TSM and FD model results very well, as shown in Figs. 9(a) and 9(b).

Difference between the quantum model and TSM as well as the FD model, however, is expected, due to the very different settings of the models. In the quantum model, the laser field is assumed to be perpendicular to the metal surface, whereas in other models, the laser incidence (i.e., the Poynting vector) is perpendicular to the metal surface. The laser power absorption in the latter

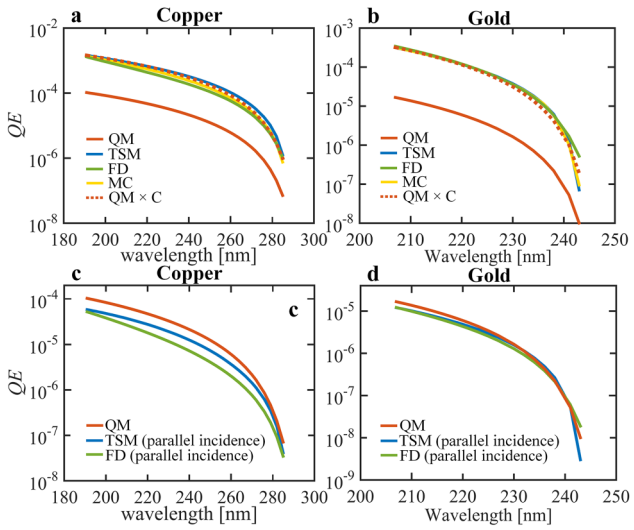

FIG. 9. (a) and (b) Quantum efficiency (QE) from the quantum model (QM) [Eq. (10)], the three-step model (TSM) [Eq. (11)], the Monte Carlo (MC) simulation based on TSM, the Fowler–DuBridge model (FD) [Eq. (12)], and the fitted QM × C (C =13.963 and 19.142 for copper and gold, respectively). (c) and (d) QE from QM [Eq. (10)], TSM [Eq. (13)] and FD model [Eq. (14)] for parallel incidence. In all the calculations, we assume the dc field $F_0 = 0$. For copper, $E_F = 7$ eV and $W_0 = 4.31$ eV;[17,18] for gold, $E_F = 5.53$ eV and $W_0 = 5.1$ eV.[22,25,26] In the QM, the laser field $F_1 = 0.01$ V/nm. In both MC simulation and TSM, $E_m = 8.6$ eV and the corresponding $\lambda_m = 2.2$ nm are used, for both copper,[15] and gold.[16] In the FD model, $a_1 = 5 \times 10^{-18}$ m^2/A[37] for copper and $a_1 = 7 \times 10^{-18}$ m^2/A for gold (by fitting to TSM). The temperature is assumed at $T = 300$ K.

case is expected to be significantly higher[33,34] and, therefore, can induce more photoelectron emission.

The case of laser field perpendicular to the metal surface may be realized when a linearly polarized laser, of the transverse electromagnetic (TEM) mode, propagates along the metal surface (i.e., parallel incidence). In this case, the laser power absorption coefficient is found to be $P_{absorption}/P_{incident} = \pi\delta_s/\lambda$,[33–35] where λ is the laser wavelength in vacuum and $\delta_s = \sqrt{2/\sigma\omega\mu_0}$ is the skin depth, with σ being the conductivity of the metal and μ_0 the vacuum permeability. By replacing $(1 - R)$ with $\pi\delta_s/\lambda$ in Eqs. (11) and (12), the TSM and FD model for parallel incidence become, respectively,

$$\mathrm{QE} = \left(\frac{\pi\delta_s}{\lambda}\right) F_{e-e} \frac{E_F + \hbar\omega}{2\hbar\omega} \left(1 - \sqrt{\frac{E_F + W}{E_F + \hbar\omega}}\right)^2, \quad \text{TSM for parallel incidence,} \tag{13}$$

$$\mathrm{QE} = a_1 \left(\frac{\pi\delta_s}{\lambda}\right) AT^2 F\left(\frac{\hbar\omega - W}{k_B T}\right), \quad \text{FD model for parallel incidence,} \tag{14}$$

where the resulted QE from both models is very close to that of the quantum model [Eq. (10)] as shown in Figs. 9(c) and 9(d). The difference between the quantum model and the other models for parallel

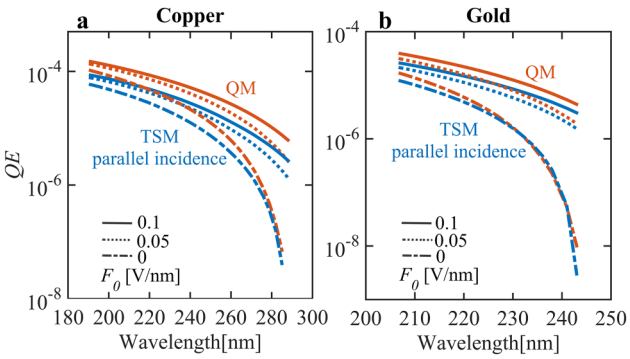

FIG. 10. Quantum efficiency (QE) from QM [Eq. (10)] and TSM for parallel incidence [Eq. (13)] under different dc fields F_0, for (a) copper and (b) gold. The other parameters are the same as in Fig. 9.

incidence could be partially explained by the assumption in the quantum model that the laser field is terminated abruptly on the metal surface, where the finite penetration of the laser field and the electron–electron scattering effect inside the metal are ignored. These volume effects become important when the laser photon energy is larger than the work function of the metal.[36] It is important to note that the QE calculation from the quantum model in Fig. 9 is only for a relatively small laser field (0.01 V/nm). Larger laser field increases QE in the longer laser wavelength range, as already displayed in Fig. 8, which cannot be predicted from either the TSM or the FD model.

Figure 10 shows the comparison of QE from our quantum model and from the TSM for parallel incidence, for both copper and gold under small dc fields (i.e., $F_0 = 0.05$ V/nm and 0.1 V/nm, respectively). The scaling of the results is in good agreement. Similar to Figs. 6 and 8, QE increases as dc field increases, especially in the longer laser wavelength, due to the combined effects of potential barrier lowering and narrowing by the dc bias. Both effects are captured in the quantum model, but only the barrier lowering effect (or Schottky effect) is included in the TSM, leading to a higher QE from the quantum model.

IV. CONCLUSION

In summary, we present a quantum model for photoemission from biased metal surfaces under the excitation of a perpendicular laser field, by solving the time-dependent Schrödinger equation exactly. The electron energy states' distribution inside the metal is assumed to follow the Fermi–Dirac distribution.

When the laser photon energy is larger than the work function of the metal, the electron emission process is dominated by single-photon absorption. Electrons are predominantly emitted from the initial energy levels in the range within one-photon energy below the Fermi level. When the laser field is small, QE is independent of the laser field strength. However, when the laser field increases (≥0.1 V/nm), QE increases with laser field strength in the longer laser wavelength range, which is due to the increased contributions from multiphoton absorption processes. This laser field- (or intensity-) dependent QE is not predicted by the

pre-existing photoemission models, such as the three-step model or the Fowler–DuBridge model. It is also found that applying a dc field can increase photoelectron emission, especially in the longer laser wavelength range, which agrees with previous studies.[17,18,22,26]

A comparison of QE by the quantum model and the existing classical models, i.e., the three-step model, the Fowler–DuBridge model, and the Monte Carlo simulation, shows the scaling of the QE by those models agrees well, despite the very different settings and assumptions used in the quantum model and the classical models. The QE from the quantum model can be fitted to that of the three-step model by a constant of proportionality, which counts mainly for the different laser (or photon) absorption coefficient under different configurations. By using the laser power absorption coefficient for parallel incidence on the cathode surface, the QE from the classical models and the quantum model are in good agreement.

We would like to emphasize again that the calculation presented in this work is only for a limited range of laser wavelengths when the photon energy is close to the work function of the metal, so that single-photon absorption dominates the electron emission process. The work may be extended to the multiphoton emission and optical field emission regimes[38,39,22] in a much wider range of laser wavelengths. In these regimes, our model will be compared with the more general formalism of TSM[32] to examine the increasingly important effects of multiple scattering, transverse energies, and multiphoton absorption processes.

For the single-photon dominated electron emission studied here, it is found that higher temperature increases the emission current only in the longer wavelength ranges under steady state. It is important to note that, however, laser heating of electron gas and the cathodes is a time-dependent process. Also, high laser intensities (or laser fields) are often realized using femtosecond laser pulses without damaging the metal sample.[38,40,41] Due to the large difference between heat capacity of electrons and phonons, as well as picosecond-scaled electron–phonon scattering, there is a thermal nonequilibrium between electrons and the lattice,[42–44] where the temperature of the electrons can reach up to thousands of kelvin.[44,45] It also takes as long as ∼1 ps for the electrons to reach a thermal equilibrium by electron–electron scattering, depending on the incident laser intensities.[46] Therefore, the electron system consists of both thermal electrons and non-thermal electrons,[46] where the Fermi–Dirac electron distribution may not be valid. This, in turn, is expected to change the step-like characteristics in electron distribution (e.g., Fig. 5) by having the photo-excitation occur from a significantly heated electron gas.[44] Consistent calculations of the time-evolved temperature of the electrons and lattice, electron distribution, and electron emission will be the subject of future study.

ACKNOWLEDGMENTS

This work was supported by the Air Force Office of Scientific Research (AFOSR) YIP Award (No. FA9550-18-1-0061).

APPENDIX: BRIEF DERIVATION OF THREE-STEP MODEL AND FOWLER-DuBRIDGE MODEL

A. Three-step model

Photoemission from metal surfaces is described in three sequential independent steps. First, electrons are excited to states of higher energies after absorption of photons. Next, the excited electrons move to the surface, which involves physical processes such as electron–electron scattering in metals. Finally, electrons overcome the potential barrier and escape into the vacuum, with a probability depending on their momentum and the surface potential. The quantum efficiency of photoemission from metal surfaces, defined as the ratio of the number of emitted electrons to that of the incident photons, is the product of the probability of those three steps,[17,18]

$$QE = [1 - R(\omega)] \times \frac{\int_{E_F+W-\hbar\omega}^{\infty} dE[1 - f_{FD}(E + \hbar\omega)] f_{FD}(E) \int_{\cos\,\theta_{max}(E)}^{1} d(\cos\,\theta) F_{e-e}(E, \omega, \theta) \int_0^{2\pi} d\phi}{\int_{E_F-\hbar\omega}^{\infty} dE[1 - f_{FD}(E + \hbar\omega)] f_{FD}(E) \int_{-1}^{1} d(\cos\,\theta) \int_0^{2\pi} d\phi}, \tag{A1}$$

where $R(\omega)$ is the reflectivity at frequency of ω, the laser is assumed incident perpendicular to the metal surface; $f_{FD}(E) = 1/(1 + \exp[(E - E_F)/k_BT])$ is the Fermi–Dirac function, describing the electron energy states distribution inside the metal; W is the effective work function, including the Schottky effect, which is the maximum of the Schottky potential composed of both image charge field and applied dc field F_0; $F_{e-e}(E, \omega, \theta)$ is the probability that electrons survive the e–e scatterings to reach the surface; θ is the angle between the velocity of the electron and the surface normal; and ϕ is the azimuthal angle on the surface. $\cos\,\theta_{max}(E) = \sqrt{(E_F + W)/(E_F + \hbar\omega)}$ gives the maximum angle of the electron velocity with respect to the normal of the surface, at which an electron can reach the surface and may eventually escape.

There are assumptions made to simplify the model. First, the metal is assumed to be at low temperature. Therefore, the Fermi–Dirac function can be approximated as a step function, with fully occupied states below E_F and empty states above E_F. Second, the photon energy of input laser is assumed to be near the threshold of photoemission, so that most of the emitted electrons are with velocity normal to the surface, and therefore the θ dependence of $F_{e-e}(E, \omega, \theta)$ can be ignored. Implied in Eq. (A1) is that electrons with the momentum normal to the surface greater than the critical barrier momentum may escape, which satisfies $p_\perp^2/2m > E_F + W$, where $p_\perp$ is the momentum normal to the surface. Thus, the model in Eq. (A1) can be simplified as[17,18]

$$\mathrm{QE} = [1 - R(\omega)] F_{e-e} \frac{(E_F + \hbar\omega)}{2\hbar\omega} \left[1 + \frac{E_F + W}{E_F + \hbar\omega} - 2\sqrt{\frac{E_F + W}{E + \hbar\omega}}\right], \tag{A2}$$

which is Eq. (11) in the main text, with all the terms defined therein.

B. Fowler–DuBridge model

The Fowler–DuBridge model for photoemission[9–12] are based on the following assumptions: (a) electrons inside a metal follow the Fermi–Dirac distribution, and electrons are distributed uniformly in the momentum space; (b) the probability of a photon absorbed by an electron is independent of the electron's initial energy state; (c) only the electron momentum component normal to the surface is increased by the absorption of photon; (d) an electron can escape from the surface, if the electron momentum normal to the surface is greater than the threshold determined by the metal work function; (e) the quantum efficiency is proportional to the number of electrons impinging on the surface, per unit area per unit time, whose kinetic energy associated with the momentum normal to the metal surface is greater than the work function of the metal. For the laser wavelength shorter than the threshold wavelength, the single-photon emission is dominant and multiphoton processes are ignored, which yields[9]

$$\mathrm{QE} = a_1(1-R)\frac{2}{h^3}\int_{-\infty}^{\infty}dp_x\int_{-\infty}^{\infty}dp_y\int_{p_1}^{\infty}dp_z\frac{p_z/m}{\exp\left(\frac{p_x^2+p_y^2+p_z^2}{2mk_BT}-\frac{E_F}{k_BT}\right)+1}, \tag{A3}$$

where p_x and p_y are the momentum along the metal surface, p_z is the momentum normal to the surface, $p_1 = \sqrt{2m(W+E_F-\hbar\omega)}$ is the minimum momentum normal to the surface required for an electron to overcome the potential barrier to emit, h is Planck's constant, k_B is the Boltzmann's constant, T is the electronic temperature, E_F is the Fermi energy, R is the metal surface reflectivity, $R = \left[(n_0-1)^2+k^2\right]/\left[(n_0+1)^2+k^2\right]$ when the laser is incident normal to the surface, n_0 is the refractive index, k is extinction coefficient or the imaginary part of the refractive index, and a_1 is a constant, which can be experimentally determined, $a_1 = 5\times10^{-18}\ \mathrm{m^2/A}$[37] for copper and $a_1 = 7\times10^{-18}\ \mathrm{m^2/A}$ for gold, which is obtained by fitting with TSM results.

By performing the integral in Eq. (A3), the quantum efficiency can be expressed as[9–12]

$$\mathrm{QE} = a_1(1-R)AT^2F\left(\frac{\hbar\omega-W}{k_BT}\right), \tag{A4}$$

where $A = 120\ \mathrm{A/cm^2/K^2}$ is Richardson's constant and $F(x)$ is Fowler's function, which is[9–11]

$$F(x) = \begin{cases} e^x - \frac{e^{2x}}{2^2} + \frac{e^{3x}}{3^2} - \cdots, & x < 0, \\ \frac{\pi^2}{6} + \frac{1}{2}x^2 - \left[e^{-x} - \frac{e^{-2x}}{2^2} + \frac{e^{-3x}}{3^2} - \cdots\right], & x > 0. \end{cases} \tag{A5}$$

REFERENCES

[1]N. A. Moody *et al.*, "Perspectives on designer photocathodes for x-ray free-electron lasers: Influencing emission properties with heterostructures and nanoengineered electronic states," Phys. Rev. Appl. **10**(4), 047002 (2018).
[2]K. L. Jensen, *Introduction to the Physics of Electron Emission* (Wiley Online Library, 2018).
[3]A. H. Zewail, "Four-dimensional electron microscopy," Science **328**(5975), 187–193 (2010).
[4]R. J. England *et al.*, "Dielectric laser accelerators," Rev. Mod. Phys. **86**(4), 1337 (2014).
[5]M. Gulde *et al.*, "Ultrafast low-energy electron diffraction in transmission resolves polymer/graphene superstructure dynamics," Science **345**(6193), 200–204 (2014).
[6]P. Zhang and Y. Y. Lau, "Ultrafast and nanoscale diodes," J. Plasma Phys. **82**(5), 595820505 (2016).
[7]P. Zhang, Á. Valfells, L. K. Ang, J. W. Luginsland, and Y. Y. Lau, "100 years of the physics of diodes," Appl. Phys. Rev. **4**(1), 011304 (2017).
[8]J. Lin, Y. Wong, P. Yang, Y. Y. Lau, W. Tang, and P. Zhang, "Electric field distribution and current emission in a miniaturized geometrical diode," J. Appl. Phys. **121**(24), 244301 (2017).
[9]R. H. Fowler, "The analysis of photoelectric sensitivity curves for clean metals at various temperatures," Phys. Rev. **38**(1), 45 (1931).
[10]L. A. DuBridge, "A further experimental test of Fowler's theory of photoelectric emission," Phys. Rev. **39**(1), 108 (1932).
[11]L. A. DuBridge, "Theory of the energy distribution of photoelectrons," Phys. Rev. **43**(9), 727 (1933).
[12]J. H. Bechtel, W. L. Smith, and N. Bloembergen, "Four-photon photoemission from tungsten," Opt. Commun. **13**(1), 56–59 (1975).
[13]W. E. Spicer, "Photoemissive, photoconductive, and optical absorption studies of alkali-antimony compounds," Phys. Rev. **112**(1), 114 (1958).
[14]C. N. Berglund and W. E. Spicer, "Photoemission studies of copper and silver: Theory," Phys. Rev. **136**(4A), A1030 (1964).
[15]W. F. Krolikowski and W. E. Spicer, "Photoemission studies of the noble metals. I. Copper," Phys. Rev. **185**(3), 882 (1969).
[16]W. F. Krolikowski and W. E. Spicer, "Photoemission studies of the noble metals. II. Gold," Phys. Rev. B **1**(2), 478 (1970).
[17]D. H. Dowell, F. K. King, R. E. Kirby, J. F. Schmerge, and J. M. Smedley, "In situ cleaning of metal cathodes using a hydrogen ion beam," Phys. Rev. Spec. Top. Accel. Beams **9**(6), 063502 (2006).
[18]D. H. Dowell and J. F. Schmerge, "Quantum efficiency and thermal emittance of metal photocathodes," Phys. Rev. Spec. Top. Accel. Beams **12**(7), 074201 (2009).
[19]P. Hommelhoff, Y. Sortais, A. Aghajani-Talesh, and M. A. Kasevich, "Field emission tip as a nanometer source of free electron femtosecond pulses," Phys. Rev. Lett. **96**(7), 077401 (2006).
[20]M. Pant and L. K. Ang, "Time-dependent quantum tunneling and nonequilibrium heating model for the generalized Einstein photoelectric effect," Phys. Rev. B **88**, 195434 (2013).
[21]R. Bormann, M. Gulde, A. Weismann, S. V. Yalunin, and C. Ropers, "Tip-enhanced strong-field photoemission," Phys. Rev. Lett. **105**(14), 147601 (2010).
[22]P. Zhang and Y. Y. Lau, "Ultrafast strong-field photoelectron emission from biased metal surfaces: Exact solution to time-dependent Schrödinger equation," Sci. Rep. **6**, 19894 (2016).
[23]W. Putnam, R. G. Hobbs, D. Keathley, K. K. Berggren, and F. X. Kärtner, "Optical-field-controlled photoemission from plasmonic nanoparticles," Nat. Phys. **13**(4), 335 (2017).
[24]S. V. Yalunin, M. Gulde, and C. Ropers, "Strong-field photoemission from surfaces: Theoretical approaches," Phys. Rev. B **84**(19), 195426 (2011).
[25]Y. Luo and P. Zhang, "Ultrafast strong-field photoelectron emission due to two-color laser fields," Phys. Rev. B **98**(16), 165442 (2018).

[26]Y. Luo and P. Zhang, "Analysis of two-color laser-induced electron emission from a biased metal surface using an exact quantum mechanical solution," Phys. Rev. Appl. **12**(4), 044056 (2019).
[27]M. Pant and L. K. Ang, "Ultrafast laser-induced electron emission from multi-photon to optical tunneling," Phys. Rev. B **86**(4), 045423 (2012).
[28]W. S. Truscott, "Wave functions in the presence of a time-dependent field: Exact solutions and their application to tunneling," Phys. Rev. Lett. **70**(13), 1900 (1993).
[29]J. G. Simmons, "Generalized formula for the electric tunnel effect between similar electrodes separated by a thin insulating film," J. Appl. Phys. **34**(6), 1793–1803 (1963).
[30]P. Zhang, "Scaling for quantum tunneling current in nano- and subnano-scale plasmonic junctions," Sci. Rep. **5**, 9826 (2015).
[31]S. Banerjee and P. Zhang, "A generalized self-consistent model for quantum tunneling current in dissimilar metal-insulator-metal junction," AIP Adv. **9**(8), 085302 (2019).
[32]K. L. Jensen *et al.*, "Multiple scattering effects on quantum efficiency and response time for cesiated metal photocathodes," J. Appl. Phys. **110**(3), 034504 (2011).
[33]S. Ramo, J. R. Whinnery, and T. Van Duzer, *Fields and Waves in Communication Electronics* (Wiley, New York, 1994), p. 508.
[34]P. Zhang, Y. Y. Lau, and R. M. Gilgenbach, "Analysis of radio-frequency absorption and electric and magnetic field enhancements due to surface roughness," J. Appl. Phys. **105**(11), 114908 (2009).
[35]C. Pérez-Arancibia, P. Zhang, O. Bruno, and Y. Y. Lau, "Electromagnetic power absorption due to bumps and trenches on flat surfaces," J. Appl. Phys. **116**(12), 124904 (2014).
[36]A. D. Gladun and P. P. Barashev, "The multiquantum photoemissive effect," Phys. Usp. **12**(4), 490 (1970).
[37]P. L. E. M. Pasmans, D. C. Van Vugt, J. Van Lieshout, G. J. H. Brussaard, and O. J. Luiten, "Extreme regimes of femtosecond photoemission from a copper cathode in a dc electron gun," Phys. Rev. Accel. Beams **19**(10), 103403 (2016).
[38]J. Girardeau-Montaut and C. Girardeau-Montaut, "Theory of ultrashort non-linear multiphoton photoelectric emission from metals," Phys. Rev. B **51**(19), 13560–13567 (May 1995).
[39]G. Herink, D. R. Solli, M. Gulde, and C. Ropers, "Field-driven photoemission from nanostructures quenches the quiver motion," Nature **483**(7388), 190–193 (2012).
[40]J. G. Fujimoto, J. M. Liu, E. Ippen, and N. Bloembergen, "Femtosecond laser interaction with metallic tungsten and nonequilibrium electron and lattice temperatures," Phys. Rev. Lett. **53**(19), 1837–1840 (1984).
[41]J.-P. Girardeau-Montaut, M. Afif, C. Tomas, A.-F. Obaton, C. Girardeau-Montaut, and K. Warda, "Ultrafast photoelectric emission from new solid materials," Appl. Surf. Sci. **106**, 451–456 (1996).
[42]S. I. Anisimov, B. L. Kapeliovich, and T. L. Perel'man, "Electron emission from metal surfaces exposed to ultrashort laser pulses," Zh. Eks. Teor. Fiz. **66**(2), 776 (1974).
[43]W. S. Fann, R. Storz, H. W. K. Tom, and J. Bokor, "Direct measurement of nonequilibrium electron-energy distributions in subpicosecond laser-heated gold films," Phys. Rev. Lett. **68**(18), 2834–2837 (1992).
[44]J. Maxson, P. Musumeci, L. Cultrera, S. Karkare, and H. Padmore, "Ultrafast laser pulse heating of metallic photocathodes and its contribution to intrinsic emittance," Nucl. Inst. Methods Phys. Res. Sec. A **865**, 99–104 (2017).
[45]Y. Zhang and J. K. Chen, "Melting and resolidification of gold film irradiated by nano- to femtosecond lasers," Appl. Phys. A **88**(2), 289–297 (2007).
[46]W. S. Fann, R. Storz, H. W. K. Tom, and J. Bokor, "Electron thermalization in gold," Phys. Rev. B **46**(20), 13592–13595 (1992).